Journal of Alloys and Compounds 513 (2012) 245–250

Contents lists available at SciVerse ScienceDirect

Journal of Alloys and Compounds

journal homepage: www.elsevier.com/locate/jallcom

Solvothermal synthesis and characterization of cobalt microcrystals with hierarchical radial structure

Mingzai Wu[a,c,*], Zhanwen Pang[a], Xiansong Liu[a], Guang Li[a], Yongqing Ma[a], Zhaoqi Sun[a], Lide Zhang[b], Xiaoshuang Chen[c]

[a] Anhui Key Laboratory of Information Materials and Devices, School of Physics and Materials, Anhui University, Hefei 230039, PR China
[b] Key Laboratory of Materials Physics, Institute of Solid State Physics, Chinese Academy of Sciences, Hefei 230031, Anhui, PR China
[c] The Shanghai Institute of Technical Physics of the Chinese Academy of Sciences, Shang 200083, PR China

ARTICLE INFO

Article history:
Received 23 July 2011
Received in revised form 8 October 2011
Accepted 11 October 2011
Available online 30 October 2011

Keywords:
Microcrystal
Synthesis
Morphologies
Magnetic properties

ABSTRACT

Three-dimensional (3D) hierarchical cobalt microcrystals composed of well-aligned dendrites radiating from the shaft axis were prepared using cobalt chloride hexahydrate as starting materials via a facile hydrothermal route. The structures and morphologies of products were investigated by X-ray diffractometer (XRD), field emission scanning electron microscopy (FESEM) and high resolution transmission electron microscopy (HRTEM) measurements. It was found that the dosages of ethylenediamine, sodium hydrate played an important role in the morphology control of the final products. A unique growth mechanism for the radial cobalt microcrystal was tentatively discussed, which offers a fresh and possible solution to the design and fabrication of materials with hierarchical structure. Additionally, Magnetization measurements revealed that the products exhibited ferromagnetic characteristics with a saturation magnetization of 151.7 emu/g and a coercivity of 355.8 Oe at room temperature. The result shows a potential application in ferrofluids and other related magnetic application.

1. Introduction

Recently, there has been growing interest in the architectural control of microstructures with specific dimensions and well-defined shapes because of their importance in the morphology-dependent properties and the capability of constructing next generation devices by the "bottom-up" approach [1–3]. The synthesis of precise-shape control and spatial pattern of a number of novel micro/nanostructures with various superstructures has been reported [4–7]. For example, dendrites of $FeNi_3$ were reported via a solvothermal synthesis in the absence of surfactants and the growth mechanism was discussed based on the diffusion-limited aggregation (DLA) model [8]. Dendrites of nickel microstructures were synthesized via a solution route. Magnetic field-induced aggregation and limited diffusion were used to explain the formation of dendrite-like nickel [9]. Moreover, sisal-like cobalt superstructures with novel turreted branches were fabricated through a solvothermal system and Ostwald ripening mechanism was believed to be responsible for the formation of sisal-like cobalt superstructures [10]. Despite the achieved progress in the controllable synthesis of hierarchical structures, the structural design and tunable fabrication of a broad range of well-defined and controllable morphologies is still desired.

Meanwhile, much attention has been paid to magnetic nanoparticles due to their novel physical and chemical properties [11–13]. Among magnetic metal nanoparticles, cobalt particles possess more outstanding magnetic properties and have potential applications in many areas including ferrofluids, biomedical systems, catalysts, optical and mechanic devices, high-density magnetic recording media [14–23]. The synthesis of cobalt particles with various morphologies has been reported including nanowires [24,25], nanorods [26], epitaxial film [27], platelets [28], rings [29], flowers [30] and chain-like structures [31,32]. For example, it has been reported recently that magnetic cobalt nanoparticles can self-assemble into rings through dipolar interactions, when dispersed under appropriate conditions, and show bistable flux closure states at ambient temperature [29]. Sphere-like and flower-like cobalt nanostructures with sharp petals were successfully synthesized via a facile liquid-phase reduction method [30]; while chainlike cobalt nanostructures composed of submicro spheres could be obtained with the aid of polyvinyl pyrrolidone (PVP) in ethylene glycol solution [32]. However, up to now, reports on the synthesis of hierarchical radial cobalt superstructures through an aqueous reduction strategy under mild conditions is still lacked.

In this paper, we present the synthesis of 3D radiated cobalt microcrystals with dendrites as the assembled unit via a facile

* Corresponding author at: Anhui Key Laboratory of Information Materials and Devices, School of Physics and Materials, Anhui University, Hefei 230039, PR China. Tel.: +86 551 5107237; fax: +86 551 5107237.
E-mail address: mingzaiwu@gmail.com (M. Wu).

0925-8388/$ – see front matter.
doi:10.1016/j.jallcom.2011.10.030

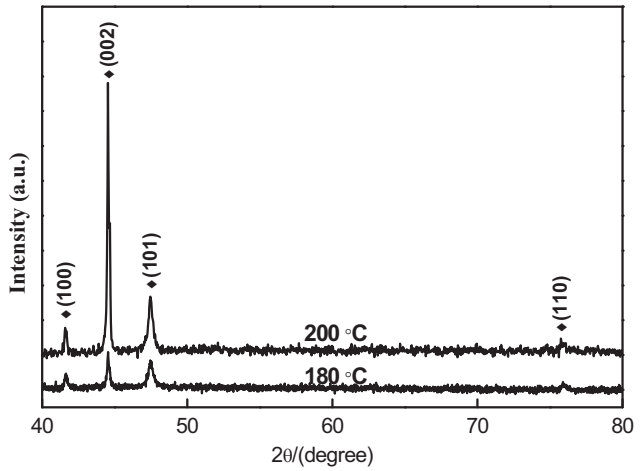

Fig. 1. XRD patterns of the prepared samples for the reaction temperatures of 180 °C and 200 °C for 4 h with $CoCl_2 \cdot 6H_2O$ (2 mmol), NaOH (3 mmol), 1.0 ml of ethylenediamine and 1.0 ml of hydrazine.

hydrothermal process. The influences of temperature, dosage of sodium hydroxide and ethylenediamine on the morphology of the products have been investigated. Based on the experiment results, a fresh and new formation mechanism is proposed. Furthermore, the magnetic behavior of the cobalt microcrystal is also studied.

2. Experimental

All the reagents are analytical grade and used as received. In a typical procedure, 0.476 g (2 mmol) of $CoCl_2 \cdot 6H_2O$ and 1.2 g of NaOH (3 mmol) were first dissolved in 30 ml of distilled water under magnetic stirring. After intensive stirring of 10 min, 1.0 ml of ethylenediamine and 1.0 ml of hydrazine were dropwise added into the above mixed solution, followed by the continual vigorous stirring for 15 min. The mixed solution was then transferred to a 50 ml Teflon-lined autoclave, which was kept at 200 °C for 4 h, and cooled to room temperature naturally. The resulted black product was collected by centrifugation, washed several times with ethanol and distilled water, and then dried at 60 °C for 12 h. Contrast experiments were carried out by adjusting the dosage of NaOH (0.6–2.4 g) and ethylenediamine (0–10 ml) with other reaction parameters unchanged.

The microstructures and morphologies of these samples were characterized by X-ray powder diffraction (XRD) using an 18 kW advanced X-ray diffractometer with Cu Kα radiation (λ = 1.54056 Å), scanning electron microscopy (SEM) and transmission electron microscopy (TEM). Magnetic hysteretic loop was measured on a vibrating sample magnetometer (VSM, BHV-55) at room temperature.

3. Results and discussion

The XRD patterns of the as-obtained cobalt crystals synthesized at different temperature for 4 h with $CoCl_2 \cdot 6H_2O$ (2 mmol), NaOH (3 mmol), 1.0 ml of ethylenediamine and 1.0 ml of hydrazine are shown in Fig. 1. All the diffraction peaks can be indexed to hcp-Co, consistent with the standard JCPDS card No. 05-0727. With the increase of the reaction temperature, the intensities of all the diffraction peaks are enhanced, indicating that the higher temperature favors the crystallization of cobalt phase. At 200 °C, the relative intensity ratios of the peak of (0 0 2) to that of (1 0 0), and (1 0 1) are much higher than those at 180 °C, suggesting the preferential growth of (0 0 1) planes. However, it is found that the reaction time and the dosages of ethylenediamine, sodium exerted less influence on the products' crystallization in terms of XRD pattern characterization, which were not shown here.

Fig. 2 shows the typical SEM and TEM images for the products synthesized at 200 °C for 4 h with $CoCl_2 \cdot 6H_2O$ (2 mmol), NaOH (3 mmol), 1.0 ml of ethylenediamine and 1.0 ml of hydrazine. Due to the products' giant size (about 15 μm in size), Fig. 2a shows only a SEM image of an overall radial microstructure composed of many dendrites, radiating from the centre with a length of 6 μm and a width of about 3 μm. The inset in Fig. 2a shows the enlarged top view of the sample. Interestingly, these dendrites serve as assembling units and grow into a quasi-flower microstructure from the same centre in a hexagonal symmetrical way. The microcrystal size is so big that HRTEM image can only be carried on a single dendrite, as shown in Fig. 2b. Fig. 2c–e shows the HRTEM lattice fringes taken from the areas labeled with 1–3 in Fig. 2b, respectively. The perfect fringes reveal the single crystal feature of the dendrite structures. Furthermore, the planar space of lattice fringes is evaluated to be 0.20 nm, and 0.22 nm (as shown in Fig. 2c–e), consistent with the (0 0 2) and (1 0 0) planes of hcp-Co. The selected-area electron diffraction (SAED) pattern shown in Fig. 2f corresponding to the area labeled with 2 further confirms the dendrite to be single crystalline, and the diffraction spots are indexed as (0 1 0) and (1 0 0) planes. Based on the planar space of lattice fringes and the indexed diffraction spots, the growth directions of the main branch and leaves of the dendrite were supposed to be along [0 0 1] direction, which agrees well with the XRD result.

It was reported that the morphology of the products was dependent on the competition between crystal nucleation and crystal growth, and the pH value was supposed to exert an impact on both the rates of crystal nucleation and crystal growth [8,33]. Here, we show our SEM images of the samples obtained at various dosages of NaOH in Fig. 3. When the dosage of NaOH is 0.6 g, incomplete leaf-like structures dominate and no radial structures are observed, as shown in Fig. 3a. With the increase of NaOH dosage to 1.0 g, the morphology of the product evolves into a perfect radial pattern, composed of some dendrite structures radiating from the same centre as shown in Fig. 3b. The venations of these dendrite crystals could be clearly distinguished. Interestingly, when the dosage of NaOH is increased to 2.4 g, the venations of dendrite crystals disappear and the sheet-like structures with saw-like edges radiate from the same centre, as shown in Fig. 3c.

It has been reported that the dosage of ethylenediamine is able to control the reaction rate and directly related to the formation of crystals [34]. Here, the controlled experiments are carried out in order to investigate the relationship of the dosage of ethylenediamine and the morphologies of crystals. Fig. 4 shows the SEM images of the as-obtained cobalt crystals synthesized with different dosages of ethylenediamine at 200 °C for 2 h. In the absence of ethylenediamine, the as-obtained samples are composed of saw-like flakes with the main backbone of dendrite, as shown in Fig. 4a. When the dosage of the ethylenediamine was 1 ml, flower-like microstructures were obtained, with leaf–like dendrites radiating from the same centre, as shown in Fig. 4b. When the ethylenediamine dosage was further increased to 10 ml, the flower-like products grew very heavy with many dendrite-like leafs radiating from the same centre. In fact, ethylenediamine played two important roles in the growth process. One is the coordination agent. It coordinates with Co^{2+} and form the stable complexing ions $[Co(NH_2CH_2CH_2NH_2)_2]^{2+}$, which reduces the concentration of free Co^{2+} ions in solution. As a result, the reduction of Co ions can be limited to a relatively slow rate, which favors the anisotropic growth of crystals. The other is surfactant [12]. Ethylenediamine molecules would be selectively adsorbed on certain crystal faces with lower surface energy. With the increase of ethylenediamine dosage, the equilibrium constant for the adsorption of ethylenediamine molecules on some crystal faces of cobalt may be changed, resulting in the changes of the growth rate and the morphologies of the final products.

The morphological changes induced by the alkalinity have been reported by many groups. For example, $La_{0.5}Ba_{0.5}MnO_3$ products with different morphologies (flowerlike, microcube, and nanocube structures) have been synthesized via the adjustment of reaction solution alkalinity [33]. The formation of single crystalline $FeNi_3$ dendrites has a great relationship with the concentration of NaOH of the solution [8]. In fact, the morphological changes

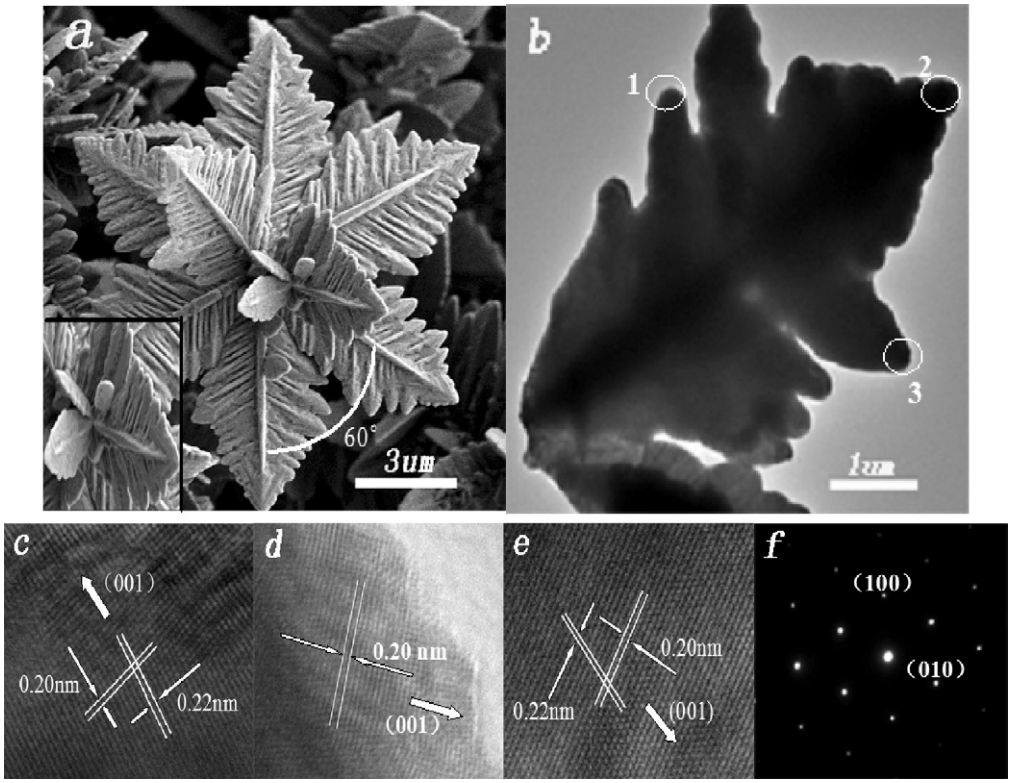

Fig. 2. (a) SEM images of the as-prepared products; (b) TEM image of a single dendrite structure. (c–e) High-resolution TEM images recorded in different part labeled by the circle in (b). (f) Electron diffraction image of the as-prepared products. (The dosage of NaOH was 1.2 g and the ethylenediamine was 1 ml.)

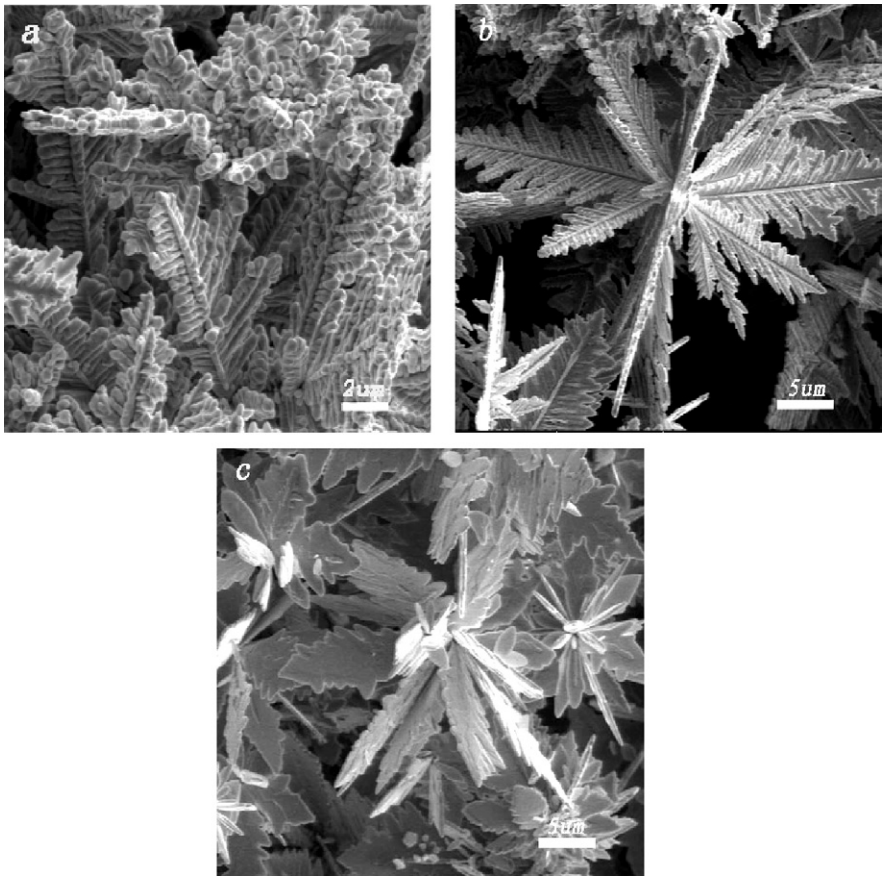

Fig. 3. SEM images of the sample prepared at 200 °C with $CoCl_2 \cdot 6H_2O$ (2 mmol), 1.0 ml of ethylenediamine and 1.0 ml of hydrazine and different dosage of sodium hydroxide: (a) 0.6 g; (b) 1.0 g; (c) 2.4 g. (The reaction time was 4 h.)

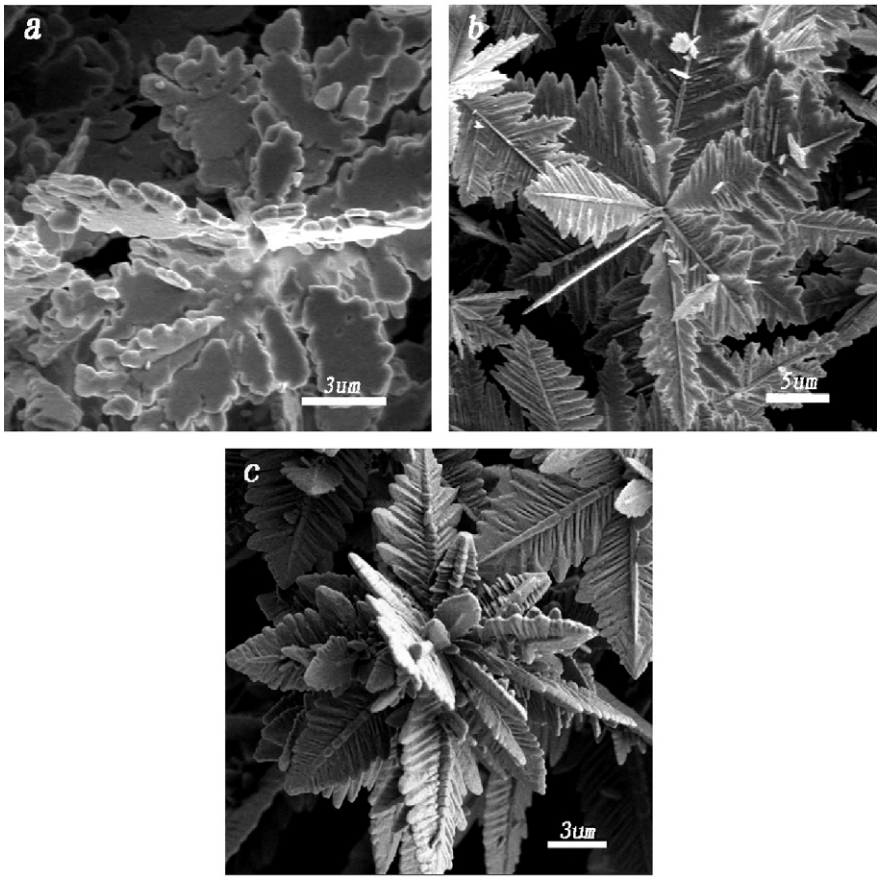

Fig. 4. SEM images of the sample prepared at 200 °C with $CoCl_2{\cdot}6H_2O$ (2 mmol), NaOH (3 mmol) and 1.0 ml of hydrazine and different dosage of ethylenediamine: (a) 0 ml; (b) 1 ml; (c) 10 ml. (The reaction time was 2 h.)

induced by the dosage of NaOH and ethylenediamine could be explained based on the fact that the dosage of NaOH affects the reaction kinetics through tuning the dissolution–deposition equation of $[Co(NH_2CH_2CH_2NH_2)_2]^{2+}$. According to Peng's theory, the high chemical potential generated by a high monomer concentration in the growth solution favors the growth along a certain direction [35]. In our system, the following reaction occurs

$$Co^{2+} + 2NH_2CH_2CH_2NH_2 \rightarrow [Co(NH_2CH_2CH_2NH_2)_2]^{2+}$$

$$2[Co(NH_2CH_2CH_2NH_2)_2]^{2+} + mN_2H_4 + 4OH^- \rightarrow 2Co + N_2\uparrow + (m-1)N_2H_4 + 4H_2O$$

Firstly, complexes $[Co(NH_2CH_2CH_2NH_2)_2]^{2+}$ are formed, and governed by the cationic/anionic mixture reaction system. Then, these complex ions are reduced to cobalt nuclei under alkaline conditions. The higher the concentration of OH^- is, the larger the number of cobalt crystal nucleus in the solution is. When the concentration of OH^- is high enough, the produced cobalt nucleus can be excessive, and will contribute to the disappearance of the venations of dendrite crystals to an extent, as shown in Fig. 3c. The viscosity enhancement of the solution should be the main reason for the formation of plate-like cobalt microstructure, as described by the Goddard–Miller equation [36]

$$\eta = \eta_0 \exp(2.5\Phi)$$

where η_0 is the viscosity of water, and Φ is the sodium hydroxide concentration. The increase of the sodium hydroxide concentration leads to the exponential increase of solution viscosity and the diffusion limitation of cobalt nuclei. Finally, the formation of plate-like cobalt structures is caused [8,33,35].

In order to further understand the growth evolution of the cobalt microcrystals, the effect of the reaction time (2 h, 4 h and 8 h) is investigated. Interestingly, a few snow-like structures can be obtained at these three reaction times. Fig. 5a shows a representative snow-like microstructure with a perfect hexangular symmetry feature obtained at 200 °C for 2 h, as shown in Fig. 5b. The short reaction time implies that the assembling process is very quick. The formation of snow-like structure is supposed to be an inevitable intermediate stage in our system. Based on the above SEM results, a possible mechanism for the growth of radial structure is proposed as shown schematically in Fig. 6.

Based on nucleation thermodynamics and reaction balance constant, particle formation depends on the ratio between nucleation and nuclei growth [37]. At the initial step of the reaction, a few small cobalt nucleuses are formed due to the hydrate hydrazine reduction. These nucleuses attract some neighboring newly reduced cobalt particles and form the trunk of cobalt microstructures (served as magnetic body). On the trunk surfaces, smaller particles are further attracted, begin to grow and finally emerge at 60 angles with respect to the trunk. With the proceeding of the reaction, the dendrite-like microstructures are formed. Under the synergistic effects of interparticles' magnetostatic interaction and diffusion-limited aggregation (DLA) induced by the NaOH, some early formed cobalt nuclei tend to be adsorbed on heterogeneous nucleation sites to reduce both the magnetic anisotropic energy and the surface energy and grow into the basic framework of hexangular snowflake microstructures with dendrite-like leafs, similar to the reports on the formation of dendrite Ag structures [38–40]. The

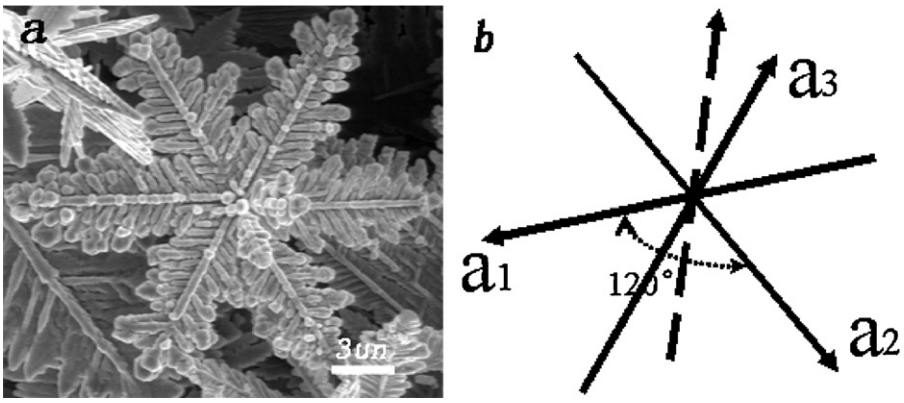

Fig. 5. (a) SEM images of snow-like structure obtained at 200 °C for 2 h with $CoCl_2{\cdot}6H_2O$ (2 mmol), NaOH (3 mmol), 1.0 ml of ethylenediamine and 1.0 ml of hydrazine. (b) Crystal shafts of hexagonal system.

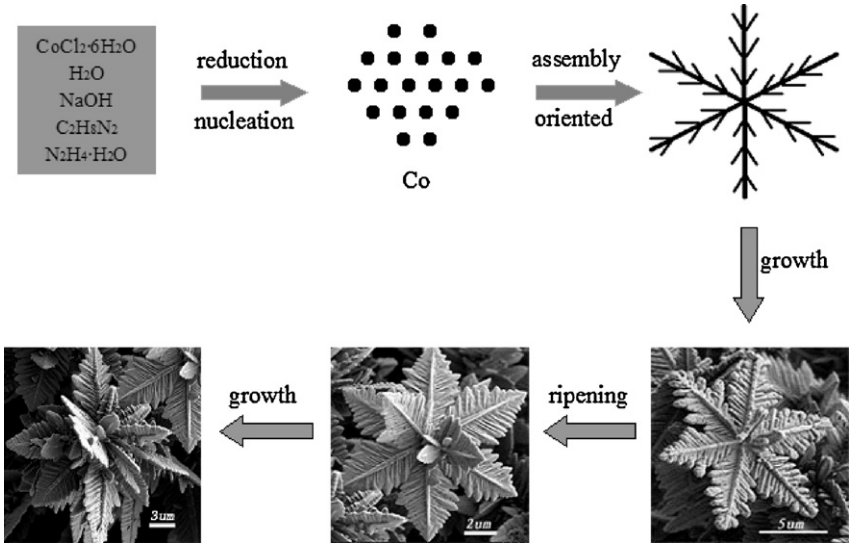

Fig. 6. Schematic illustration of the possible formation process of the products.

growth velocity of c axis [0 0 0 1], is much larger than that in the ab plane. Thus, the continual growth can be induced along the c axis. It is the fact that the size of the ripened radial structure is bigger than that of the snowflake one, which supports the conclusion that the radial structures grow from the snowflake ones. With the consumption of the reactants and ethylenediamine, the equilibrium constant of ethylenediamine molecules binding with certain crystal faces of cobalt, may be changed, leading to the changes of the growth rate of cobalt crystal faces. Ostwald ripening process can occur. It is proposed that the formation of trunk part and the growth of the microstructures are a directed assembled process followed by the Ostwald ripening, different from the reported traditional mechanism in Ref. [10]. Fig. 7 shows the detailed evolution process. The novel growth mechanism offers a unique and possible solution to the design and preparation of materials with advanced functionalities. More details about the growth mechanism are still underway.

The magnetic properties are investigated by the magnetization dependence of applied fields at 300 K, as shown in Fig. 8. The sample synthesized under the conditions of 200 °C for 4 h, 0.476 g of $CoCl_2{\cdot}6H_2O$, 1.2 g of NaOH, 1.0 ml of ethylenediamine, 1.0 ml of hydrazine is found to possess the hysteretic behavior. The result reveals that the Co microstructures are ferromagnetic. The inset is the magnetized hysteretic loops at low applied field. The values of saturated magnetization (M_S), remnant magnetization (M_r), and coercivity (H_c) are 151.7 emu/g, 22.42 emu/g, and 355.8 Oe, respectively. The saturation magnetization (M_S) for the sample is much close to the corresponding values for the bulk cobalt (M_S = 168 emu/g). The much higher

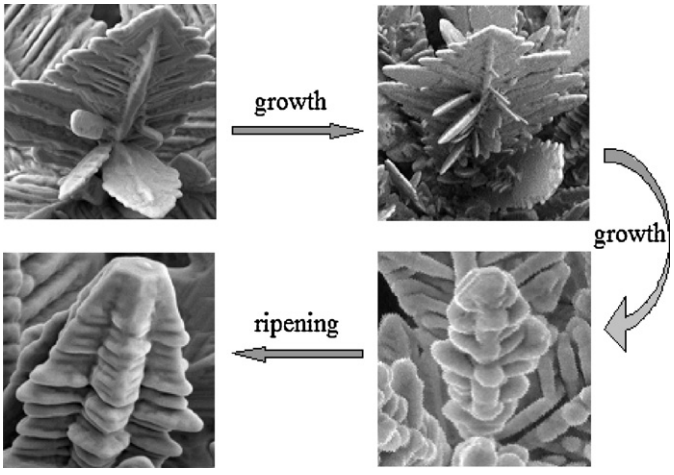

Fig. 7. Schematic illustration of the possible formation process of the trunk structure.

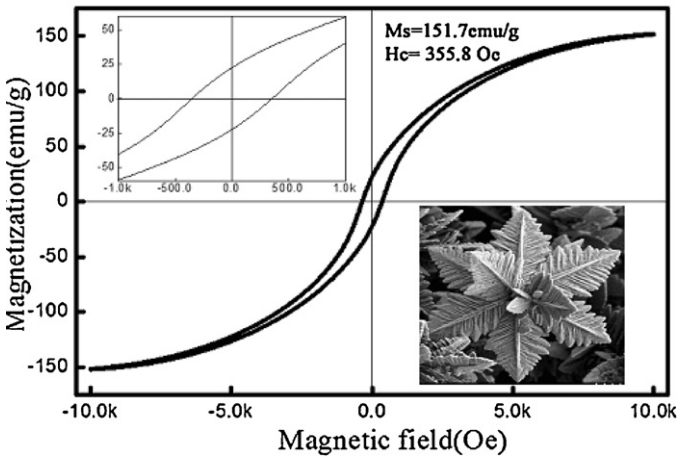

Fig. 8. Room temperature hysteretic loops of the sample obtained at 200 °C for 4 h with $CoCl_2 \cdot 6H_2O$ (2 mmol), NaOH (3 mmol), 1.0 ml of ethylenediamine and 1.0 ml of hydrazine.

coercivity value than that of the bulk (ca. 10 Oe) [41] may result from the shape anisotropy of our novel cobalt structures.

4. Conclusions

In summary, 3D cobalt microcrystals of radiated structures with a size about 15 μm were successfully synthesized by a simple hydrothermal reaction. The 3D Co superstructures are comprised of dozens of well-aligned cobalt dendrites radiating from the centre. The dosages of NaOH and ethylenediamine played an important role in the control of size, morphology, and structure of the products. The magnetic measurement shows that cobalt microcrystals have a higher coercivity. The value of the saturated magnetization (M_S) and coercivity (H_C) was 151.7 emu/g and 355.8 Oe, respectively. Additionally, this work provides a facile and effective strategy to the preparation of novel cobalt structures with tunable morphologies.

Acknowledgements

This work was financed by the 211 project of Anhui University, National Natural Science Foundation of China (50901074, 60976092, 11174002, 50672001), Anhui Provincial Natural Science Fund (11040606M49), Higher Educational Natural Science Foundation of Anhui Province (KJ2010A012) and Innovation Project of Anhui University Graduate Education (yqh090010).

References

[1] X.J. Xu, X.S. Fang, H.B. Zeng, T.Y. Zhai, Y. Bando, D. Golberg, Sci. Adv. Mater. 2 (2010) 273.
[2] D. Vennerberg, Z.Q. Lin, Sci. Adv. Mater. 3 (2011) 26.
[3] Y.S. Chen, Y.L. Wei, P.M. Chang, L.J. Ye, J. Alloys Compd. 509 (2011) 5381.
[4] Y. Tian, G.M. Hua, W. Xu, N. Li, M. Fang, L.D. Zhang, J. Alloys Compd. 509 (2011) 724.
[5] C.H. Ye, Sci. Adv. Mater. 2 (2010) 365.
[6] M.Z. Wu, Y. Xiong, Y.S. Jia, K. Zhang, Q.W. Chen, Appl. Phys. A 81 (2005) 1355.
[7] X.L. Shi, M.S. Cao, J. Yuan, Q.L. Zhao, Y.Q. Kang, X.Y. Fang, Y.J. Chen, Appl. Phys. Lett. 93 (2008) 183118.
[8] X.M. Zhou, X.W. Wei, Cryst. Growth Des. 9 (2009) 7.
[9] J. Ye, Q.W. Chen, H.P. Qi, N. Tao, Cryst. Growth Des. 8 (2008) 2465.
[10] Z.G. An, J.J. Zhang, S.L. Pan, Mater. Chem. Phys. 123 (2010) 795.
[11] Y.J. Chen, M.S. Cao, Q. Tian, T.H. Wang, J. Zhu, Mater. Lett. 58 (2004) 1481.
[12] M.S. Cao, R.G. Wang, X.Y. Fang, Z.X. Cui, T.J. Chang, H.J. Yang, Powder Technol. 115 (2001) 96.
[13] S. Shiv Shankar, S. Deka, Sci. Adv. Mater. 3 (2011) 169.
[14] A. Zarian, A.I. Zad, A. Dolati, Opt. Commun. 274 (2007) 471.
[15] K.T. Nam, D.W. Kim, P.J. Yoo, C.Y. Chiang, N. Meethong, P.T. Hammond, Y. Chiang, A.M. Belcher, Science 312 (2006) 885.
[16] H. Kim, M. Achermann, L.P. Balet, J.A. Hollingsworth, V.I. Klimov, J. Am. Chem. Soc. 127 (2005) 544.
[17] M.C. Parry, G. Bhabra, A. Sood, F. Machado, L. Cartwright, M. Saunders, E. Ingham, R. Newson, A.W. Blom, C.P. Case, Biomaterials 31 (2010) 4477.
[18] W.Q. Qin, C.R. Yang, X.H. Ma, S.S. Lai, J. Alloys Compd. 509 (2011) 338.
[19] J. Krzystek, D.C. Swenson, S.A. Zvyagin, D. Smirnov, A. Ozarowski, J.J. Telser, J. Am. Chem. Soc. 132 (2010) 5241.
[20] L.P. Zhu, H.M. Xiao, W.D. Zhang, Y. Yang, S.Y. Fu, Cryst. Growth Des. 8 (2008) 1113.
[21] V.F. Puntes, K.M. Krishnan, A.P. Alivisatos, Science 291 (2001) 2115.
[22] S. Okamoto, L.D. Eltis, Metallomics 3 (2011) 963.
[23] R. Rungsawang, J. da Silva, C.P. Wu, E. Sivaniah, A. Ionescu, C.H.W. Barnes, N.J. Darton, Phys. Rev. Lett. 104 (2010) 255703.
[24] A. Cortés, R. Lavín, J.C. Denardin, R.E. Marotti, E.A. Dalchiele, P. Valdivia, H. Gómez, J. Nanosci. Nanotechnol. 11 (2011) 3899.
[25] H. Cao, Z. Xu, H. Sang, D. Sheng, C. Tie, Adv. Mater. 13 (2001) 121.
[26] F. Dumestre, B. Chaudret, C. Amiens, M.C. Fromen, M.J. Casanove, P. Renaud, P. Zurcher, Angew. Chem. Int. Ed. 41 (2002) 4286.
[27] N.L. Yakovlev, H. Chen, K. Zhang, J. Nanosci. Nanotechnol. 11 (2011) 2575.
[28] M.H. Pan, H. Liu, J.Z. Wang, J.F. Jia, X.Q.K. Xue, J.L. Li, S. Qin, U.M. Mirsaidov, X.R. Wang, J.T. Markert, Z. Zhang, C.K. Shih, Nano Lett. 5 (2005) 87.
[29] A. Wei, T. Kasama, R.E. Dunin-Borkowski, J. Mater. Chem. (2011), doi:10.1039/C1JM11916H.
[30] C. Wang, X.J. Han, X.L. Zhang, S.R. Hu, T. Zhang, J.Y. Wang, Y.C. Du, X.H. Wang, P. Xu, J. Phys. Chem. C 114 (2010) 14826.
[31] X.L. Shi, M.S. Cao, J. Yuan, X.Y. Fang, Appl. Phys. Lett. 95 (2009) 163108.
[32] Y.J. Zhang, Q. Yao, Y. Zhang, Tie.Y. Cui, D. Li, W. Liu, W. Lawrence, Z.D. Zhang, Cryst. Growth Des. 8 (2008) 3207.
[33] P. Chai, X.J. Liu, Z.L. Wang, M.F. Lu, X.Q. Cao, J. Meng, Cryst. Growth Des. 7 (2007) 2568.
[34] L.J. Zhao, L.F. Duan, Y.Q. Wang, Q. Jiang, J. Phys. Chem. C 114 (2010) 10691.
[35] Z.A. Peng, X.G. Peng, J. Am. Chem. Soc. 123 (2001) 1389.
[36] J.D. Goddard, C. Miller, J. Fluid Mech. 28 (1967) 657.
[37] M.S. Cao, H.T. Liu, Y.J. Chen, B. Wang, J. Hu, Sci. China Ser. E-Technol. Sci. 46 (2003) 104.
[38] J.X. Fang, H.J. You, P. Kong, Y. Yi, X.P. Song, B.J. Ding, Cryst. Growth Des. 7 (2007) 865.
[39] Y.N. Zhao, M.S. Cao, H.B. Jin, X.L. Shi, X. Li, S. Agathopoulos, J. Nanosci. Nanotechnol. 6 (2006) 2525.
[40] Y.N. Zhao, M.S. Cao, H.B. Jin, L. Zhang, C.J. Qiu, Scripta Mater. 54 (2006) 2057.
[41] Q. Xie, Y.T. Qian, S.Y. Zhang, S.Q. Fu, W.C. Yu, Eur. J. Inorg. Chem. 12 (2006) 2454.